Trans. JSASS Aerospace Tech. Japan
Vol. 16, No. 2, pp. 110-115, 2018
DOI: 10.2322/tastj.16.110

Numerical Investigation of Steady and Transient Ion Beam Extraction Mechanisms for Electrospray Thrusters

By Kazuma EMOTO,[1)] Toshiyuki TSUCHIYA,[2)] and Yoshinori TAKAO[3)]

[1)]*Department of Systems Integration, Yokohama National University, Yokohama, Japan*
[2)]*Department of Micro Engineering, Kyoto University, Kyoto, Japan*
[3)]*Division of Systems Research, Yokohama National University, Yokohama, Japan*

(Received June 30th, 2017)

Electrospray thrusters are simple propulsion systems, which can be operated on nanosatellites, and it is possible to reduce components of high pressure gas systems using ionic liquid as a propellant. However, evaluations of electrospray thrusters are difficult in experiments since the size of emitter cones is on the order of micrometers. Then, the authors performed Particle-in-Cell simulations of ions in the electrospray thruster and investigated ion beam extraction mechanisms in steady and transient flows numerically. The simulation results show that steady ion beam distributions were rarely affected by ion species. On the other hand, it was clarified that a jet affected the ion beam profiles. In addition, the authors evaluated propulsion performance of the electrospray thruster, which showed a thrust of about 64 nN per emitter and a specific impulse of about 6400 s. In the transient flow, the ion beam behavior showed rapid responses when applied voltages with or without a slew rate are assumed.

Key Words: Electric Propulsion, Electrospray Thruster, Ionic Liquid, Particle-in-Cell

Nomenclature

$\boldsymbol{E}$	:	electric field
F	:	thrust
f	:	probabilistic density
g	:	gravitational acceleration
I	:	current
k_{B}	:	Boltzmann constant
m	:	mass
$\dot{N}$	:	the number of ions per second
n	:	the number of ions
q	:	charge
T	:	temperature
$\boldsymbol{v}$	:	velocity
$\boldsymbol{x}$	:	position
Δt	:	time step
ε_0	:	vacuum permittivity
π	:	circular constant
ρ	:	charge density
Subscripts		
e	:	exhaust/exit
z	:	axial direction

1. Introduction

Developments in space technology have been conducted by many countries, and some companies plan to operate hundreds of nanosatellites, whose cost is extremely low compared with large satellites. Although propulsion systems are necessary for spacecraft to maintain or change their orbits actively, conventional thrusters are too large to be mounted on nanosatellites. Therefore, there is a considerable demand for small thrusters which can be operated on nanosatellites.

Among candidates for small electric propulsion systems, electrospray thrusters can be significantly miniaturized, and their mechanisms are simpler than conventional thrusters. Figure 1 shows a bipolar operation of the electrospray thruster. The electrospray thruster consists of an emitter chip and an extractor grid, and emitter cones are wetted by ionic liquid as a propellant. By switching a voltage polarity applied to the emitter chip, both positive and negative ion beams can be extracted, and spacecraft can keep their electric neutrality without neutralizers. Since ionic liquid contains only ions without solvent, its vapor pressure is almost zero, and it is easy to store in space.[1)]

Electrospray thrusters have been already fabricated and operated in space, and many studies of electrospray thrusters were reported so far.[2-7)] However, the number of operations is still small, and optimization of electrospray thrusters is in progress. Here, the authors simulated ion beams extracted from an emitter tip using Particle-in-Cell simulations, which are often conducted in conventional plasma thrusters. In this paper,

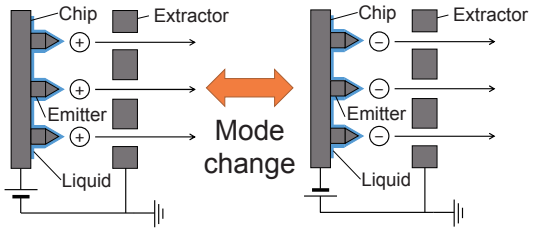

Fig. 1. Bipolar operation of electrospray thruster.

the authors focus on steady and transient flows of ion beams in electrospray thrusters, and effects of dimers and a jet are investigated as additional studies.

2. Numerical Model

2.1. Configuration

To reduce a calculation cost, the authors focused on an emitter cone and used two-dimensional cylindrical coordinates. Figure 2 shows the calculation model of the electrospray thruster. The calculation model has the same sizes and conditions as experiments by the authors.[7] The emitter cone has a shape of a pencil which is 0.07 mm in radius and 0.2 mm in height. An area surrounded by dotted lines is considered in this study. The calculation area is divided into 5 μm × 5 μm square cells.

2.2. Propellant

Figure 3 shows a chemical structural formula of EMI-BF_4 (1-ethyl-3-methylimidazolium tetrafluoroborate), which the authors chose as the propellant. A molecular of EMI-BF_4 has a cation of EMI^+ and an anion of BF_4^-. It was assumed that the ions contain only monomers or both monomers and dimers in this simulation, which were measured by Time-of-Flight spectra in experiments: EMI^+, BF_4^-, $(EMI\text{-}BF_4)EMI^+$, and $(EMI\text{-}BF_4)BF_4^-$.[8] Table 1 shows molar mass of ions considered in the simulation. In the condition containing both monomers and dimers, it was assumed that cations contained 85% monomers and 15% dimers and that anions contained 72% monomers and 28% dimers.[9]

It was assumed that ions corresponding to 1 μA are emitted from the emitter tip.[9] The number of ions emitted from the emitter tip per second $\dot{N}$ is described as

$$\dot{N} = \frac{I}{q}. \tag{1}$$

In addition, ions were given random initial velocities at the emitter tip. These velocities were assumed to satisfy an isotropic Maxwellian velocity distribution described as

$$f = \left(\frac{m}{2\pi k_B T}\right)^{\frac{3}{2}} \exp\left(-\frac{m\boldsymbol{v}^2}{2k_B T}\right), \tag{2}$$

with a temperature of 2.6 eV at the emitter tip.[10] It should be noticed that ions have probably certain angular distributions at the beginning of ion emission from ionic liquid at the emitter tip. However, there are no experimental reports regarding such distributions. Hence, we focus on the effect of the potential distributions between the electrodes on ion beam trajectories assuming the isotropic Maxwellian distribution at the emitter tip.

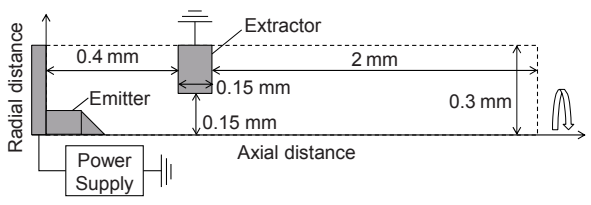

Fig. 2. Calculation model of electrospray thruster.

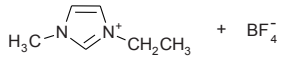

Fig. 3. Chemical structural formula of EMI-BF_4.

Table 1. Information of ions.

Ions		Molar mass (g mol^{-1})
Cation	EMI^+	111
	$(EMI\text{-}BF_4)EMI^+$	309
Anion	BF_4^-	86.8
	$(EMI\text{-}BF_4)BF_4^-$	285

2.3. Applied voltage

To study steady and transient flows, we set two types of the voltage applied to the emitter chip. In the steady flow, the applied voltage was fixed to +2 or −2 kV. In the transient flow, a bipolar pulse of ±2 kV was applied to the emitter chip. The voltage applied to the extractor grid was fixed to 0 V in both flows.

2.4. Particle-in-Cell simulation

To obtain profiles of the ion beam extracted from the emitter tip, the authors employed Particle-in-Cell simulations.[11] Firstly, positions of ions are obtained solving equations of motion described as

$$\boldsymbol{v} = \frac{d\boldsymbol{x}}{dt}, \tag{3}$$

$$\frac{d\boldsymbol{v}}{dt} = \frac{q}{m}\boldsymbol{E}. \tag{4}$$

Secondly, a charge density is calculated from the positions of ions. By using the charge density, a Poisson's equation is obtained as

$$\boldsymbol{\Delta}\phi = -\frac{\rho}{\varepsilon_0}. \tag{5}$$

Eq. (5) can be rewritten in two-dimensional cylindrical coordinates as

$$\left(\frac{\partial^2}{\partial r^2} + \frac{1}{r}\frac{\partial}{\partial r} + \frac{\partial^2}{\partial z^2}\right)\phi = -\frac{\rho}{\varepsilon_0}. \tag{6}$$

We solve Eq. (6) and obtain a new potential distribution using a successive over-relaxation (SOR) method.[12] Then, the electric field is derived by solving

$$\boldsymbol{E} = -\boldsymbol{\nabla}\phi. \tag{7}$$

We conducted a symmetric spline weighting to eliminate axisymmetric errors of the charge density on the central axis.[13] In addition, we correct the charge density using a digital smoothing algorithm to decrease a scattering of the distribution.[14]

By iterating Eqs. (3)−(7), we obtain profiles of the ion beam. Initial ions are emitted at the emitter tip every cycle before the calculation of the charge density, and the time step Δt was set to 0.1 ns.

2.5. Evaluations of thruster performance

To evaluate performance of the electrospray thruster, we calculated thrusts and specific impulses. In the evaluations, when ions just passed through the extractor grid, the values of those velocities were used since it was regarded that ions in the

downstream from the extractor grid were out of the propulsion system.

Firstly, the thrust F is calculated as a summation of the axial ion momentum mv_z divided by the time step Δt:

$$F = \frac{\sum mv_z}{\Delta t}. \tag{8}$$

Secondly, the exhaust velocity v_e is calculated as an average axial velocity v_z:

$$v_e = \frac{\sum v_z}{n}, \tag{9}$$

where n is the number of ions which passed through the extractor grid. Then, the specific impulse I_{sp} is calculated as the exhaust velocity v_e divided by the gravitational acceleration g:

$$I_{sp} = \frac{v_e}{g}. \tag{10}$$

Although these calculations are just simple estimates, we can numerically evaluate the electrospray thruster.

2.6. State of ionic liquid near emitter tip

It was reported that a column of ionic liquid might be formed at the emitter tip when ions are extracted, which is called jet.[15,16] Figure 4 shows a schematic of the ionic liquid with the jet near the emitter tip, where the electrospray phenomena are divided into three states: cone, jet, and spray. In the state of the cone, ionic liquid has a conical shape along the emitter cone as a liquid phase. In the state of the jet, ionic liquid is extracted by a strong electric field as a liquid phase and has the column shape. In the state of the spray, ionic liquid exists as particles, such as monomers, dimers, or droplets.

If the jet is formed, a radial electric field is increased near the jet since the jet has a high voltage which is the same value as the emitter chip. Then, it is expected that ions are accelerated by the jet in the radial direction and that a half angle of the ion beam is increased.

Here, we conducted both the simulation with and without the jet and compared these results. It was assumed that the jet existed only on the central axis and that the potential of the jet was the same value as the emitter chip. It is also assumed that ions were extracted from the jet tip and that a length of the jet was 0.1 mm.

2.7. Slew rate

In experiments, applied voltages have a slew rate (<1200 V μs^{-1}). Here, we simulated ion beams when the voltage rose from 0 to +2 kV with the slew rate to make simulations close to actual conditions. It was assumed that the ions were extracted from the emitter tip when the threshold voltage of +1.7 kV or more was applied to the emitter chip, which was an averaged value measured in previous experiments.[7)]

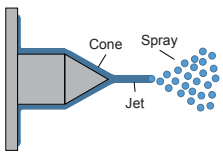

Fig. 4. State of electrospray near emitter tip.

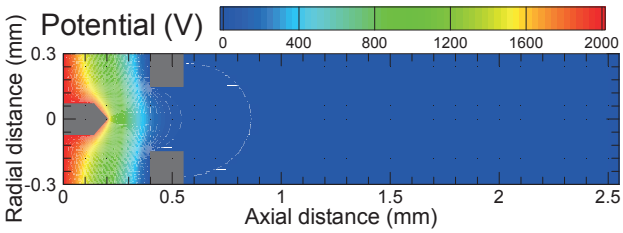

Fig. 5. Static potential distribution.

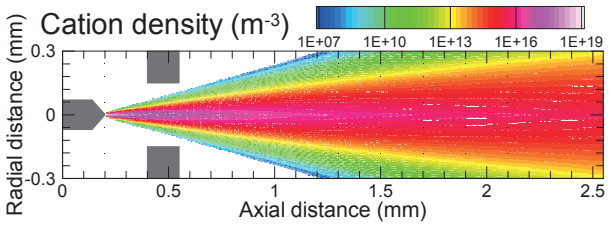

Fig. 6. Cationic monomer density distribution (only monomers).

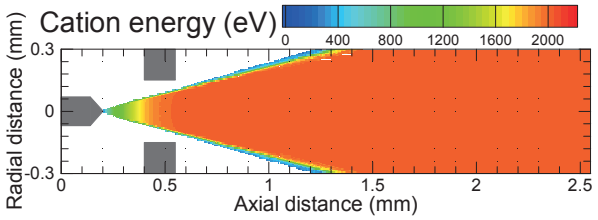

Fig. 7. Cationic monomer energy distribution (only monomers).

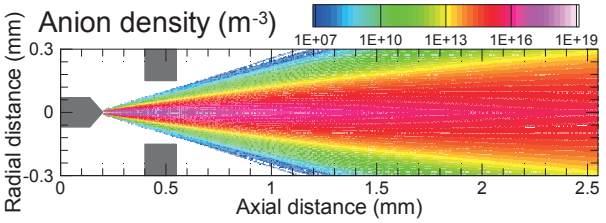

Fig. 8. Anionic monomer density distribution (only monomers).

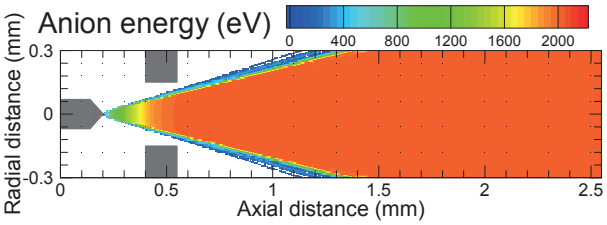

Fig. 9. Anionic monomer energy distribution (only monomers).

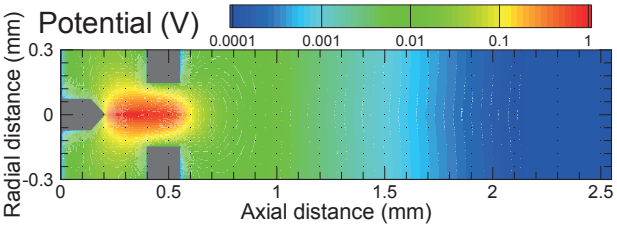

Fig. 10. Potential distribution due to space charge of cationic monomers (only monomers).

3. Results and Discussion

3.1. Steady flow

3.1.1. Static potential

Figure 5 shows a static potential distribution by the voltage applied to the emitter chip in the case of no ions in the calculation area. Here and all the other distributions are mirrored with respect to the z-axis. The potential decreases from +2 to 0 kV between the emitter chip and the extractor grid, and the potential gradient near the emitter tip was higher than the other area because of the shape of the emitter cone. It is expected that ions are accelerated by the static potential gradient although ions may be decelerated by the space charge of the ion beam. In addition, ions can be slightly accelerated in the radial direction because of a radial potential gradient due to the emitter cone.

3.1.2. Cationic monomer beam distributions

Figures 6 and 7 show the time-averaged distributions of the cationic monomer density and energy when the only cationic monomers are extracted by applying +2 kV at the emitter chip. It should be noted that the values of densities and energies are averaged over 30 μs hereafter.

The maximum value of the cationic monomer density is about 10^{19} m^{-3} near the emitter tip while a minimum value of that is about 10^{7} m^{-3} at an edge of the cationic monomer beam. A difference of the cationic monomer density is about 10^{5} m^{-3} between the center and the edge of the cationic monomer beam at the extractor grid section (z = 0.5 mm).

The energy of cationic monomers is immediately increased along the axial direction, and ions gain the energy corresponding to the applied voltage downstream of the extractor grid. On the edge of the ion beam, the time-averaged energy seems to be low since the divergence angle of the ion beam is continuously changed owing to the random initial velocities at the emitter tip.

A half angle of the cationic monomer beam is about 16.7°, which is small compared with a previous value measured in experiments.[9] However, the half angle of the ion beam depends on the initial velocity distribution, which is Maxwellian in this simulation. In the future, it is necessary to decide the initial velocity and angular distributions in more detail. We plan to use molecular dynamics simulations to study motions of ions near the emitter tip.

3.1.3. Anionic monomer beam distributions

Figures 8 and 9 show the time-averaged distributions of the anionic monomer density and energy when the only anionic monomers are extracted by applying −2 kV at the emitter chip. Anionic monomer density and energy distributions are almost the same as the results of the cationic monomer. However, anion beam profiles such as the ion density or the half angle of the beam are slightly different from the cation beam because of a difference in mass.

3.1.4. Potential due to space charge of ions

Figure 10 shows the time-averaged distribution of the potential due to space charge by cationic monomers. The potential is about 0.1–1 V near the emitter tip or the hole of the extractor grid and is smaller than about 0.1 V in the other area, such as the downstream. Since the potential of space charge is smaller than about 1 V in the whole simulation area, the potential due to space charge of cationic monomers is several orders of magnitude smaller than the static potential shown in Fig. 5. Therefore, the static potential is an important factor for the electrospray thruster and determine the ion motions dominantly while the potential due to space charge is not important, unlike conventional ion thrusters.

Table 2. Performance of ion beam (only monomers).

Ions	Thrust F (nN)	Specific impulse I_{sp} (s)
EMI^+	68.0	6026
BF_4^-	60.1	6820

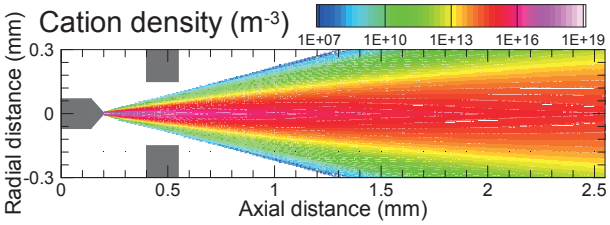

Fig. 11. Cationic density distribution focused only dimers in the mixture of monomers and dimers.

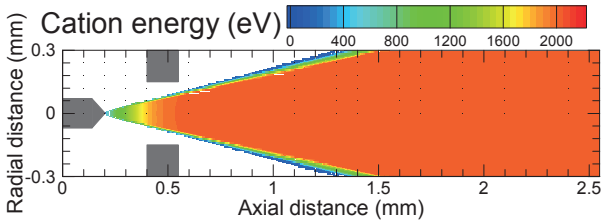

Fig. 12. Cationic energy distribution focused only dimers in the mixture of monomers and dimers.

3.1.5. Performance of electrospray thruster

Table 2 shows time-averaged propulsion performance of the cationic and the anionic monomer beam: the thrust F and the specific impulse I_{sp}. In the cation beam, the thrust was 68.0 nN, and the specific impulse was 6026 s. On the other hand, the thrust was 60.1 nN, and the specific impulse was 6820 s in the anion beam. Therefore, the electrospray thruster realizes the high specific impulse although their thrust is small. However, we focus an emitter cone in this simulation, and hundreds of emitter cones are arrayed on the emitter chip actually. Thus, electrospray thrusters will provide the thrust of hundreds micro-newton which is necessary for microsatellites to keep the station or deorbit. We have been fabricating emitter chips whose emitter pitch is 5 μm.[17,18]

3.1.6. Ion beam containing monomers and dimers

We simulated a cation beam containing both monomers and dimers extracted from the emitter tip of +2 kV. Then, we separated results of cationic dimers alone, and Figs. 11 and 12 show the time-averaged distributions of the cationic dimer density and energy. Both of distributions are almost the same as results of only monomers although the beam profiles are slightly different because of the difference in mass. Thus, ion beam profiles are not affected by ion species.

However, emissions of droplets were measured in addition to monomers and dimers in experiments.[19] Thus, ion beam

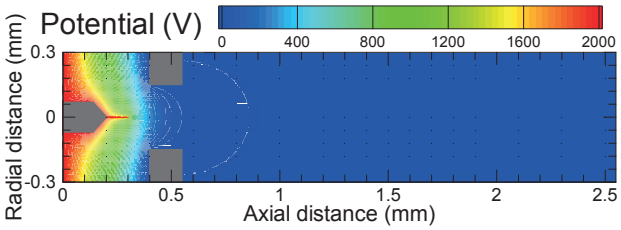

Fig. 13. Static potential distribution with jet.

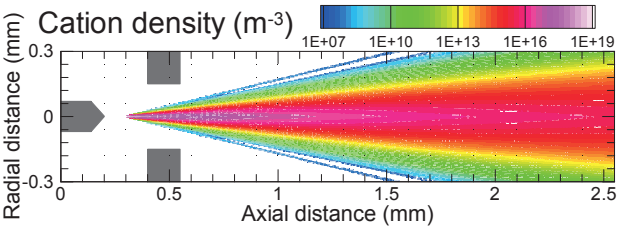

Fig. 14. Cationic monomer density distribution with jet.

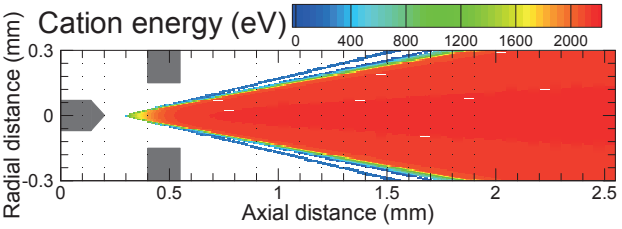

Fig. 15. Cationic monomer energy distribution with jet.

profiles containing droplets may be different from results of monomers and dimers since droplets have significantly larger mass. Simulations of the ion beam containing droplets is left for our future work.

We also simulated an anion beam containing both monomers and dimers extracted from the emitter tip of −2 kV and obtained almost the same distributions as the cationic dimer beam (not shown here).

3.1.7. Ion beam with jet

Figure 13 shows the distribution of the static potential when an existence of the jet was assumed. Compared with Fig. 5, no significant change is seen in the static potential distribution while the potential near the jet increased. Hence, it is expected that ions which are extracted from the jet tip are more accelerated than without the jet in the radial direction.

Figures 14 and 15 show the time-averaged distributions of the cationic monomer density and energy with the jet. Here, we assumed that ions contained only monomers. Since ions were assumed to be extracted from the jet tip, a starting point of the cationic monomer beam was only the length of the jet away from the emitter tip. The half angle of the cationic monomer beam is estimated at 12.1°, which is lower than that of the ion beam without the jet. This result is unexpected, and the reason is that the distance between the jet tip and the extractor grid was short compared with no jet, and thus, the axial component of the electric field dominates over its radial component. In addition, we obtained almost the same results in anionic monomers when the emitter chip is applied at −2 kV with the jet.

In the jet model, the consideration of the initial velocity distribution at the emitter tip is not conducted yet, and additional studies are required. In addition, the jet model may be insufficient since it was assumed that the jet only existed along the central axis without a thickness and that ions were extracted only from the jet tip. In the future, we will employ the jet which has the finite thickness.

3.2. Transient flow

3.2.1. Switching of applied voltage by step function

Figure 16 shows the temporal variations of the applied voltage and the ion beam current. It was assumed that the ions consist of only monomers for simplicity. When the voltage of +2 kV is applied to the emitter chip, cations are extracted from the emitter tip. On the other hand, when the voltage of −2 kV is applied to the emitter chip, anions are extracted from the emitter tip. After the applied voltage was switched from +2 to −2 kV, the ion beam current responded quickly and began to extract anions, where a switching time of the ion current was about 20 ns. Owing to this short response time, the switching time would not matter in the operation of the electrospray thruster. One of the reasons for the quick response is that ions obtain the energy of 2 keV and passed through the extractor grid for only several nano seconds because of the short distance of 0.35 mm between

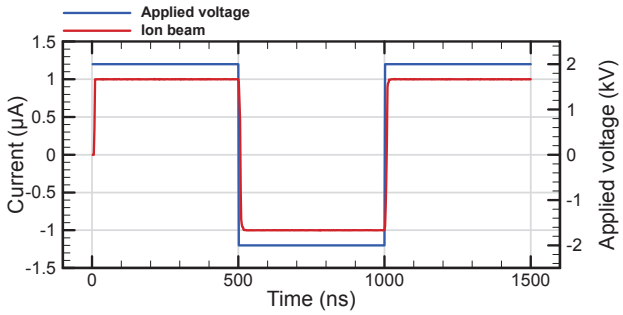

Fig. 16. Temporal variation of applied voltage and ion beam current (Step function).

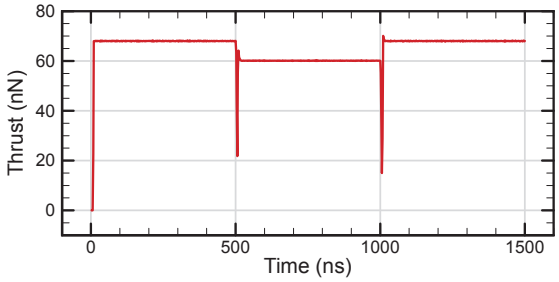

Fig. 17. Temporal variation of thrust (Step function).

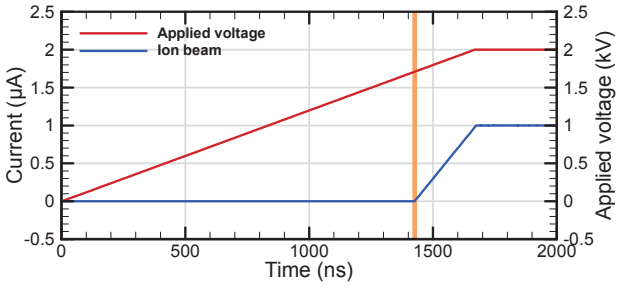

Fig. 18. Temporal variation of applied voltage and ion beam current with slew rate.

the emitter tip and the extractor grid.

Figure 17 shows the temporal variation of the thrust. The thrust of cations is higher than that of anions since the cation mass is larger than the anion mass. After the thrust dropped for a moment when the applied voltage was switched, the thrust immediately returned to the steady state. However, the applied voltage has a slew rate in experiments, and it is expected that the thrust changes according as the switching voltage.

3.2.2. Initial rise of ion beam with slew rate

Figure 18 shows the temporal variations of the applied voltage and the ion beam current with the slew rate. It was assumed that ions contained only monomers and that the slew rate was 1200 V μs^{-1} which can be realized in experiments. It is noted that an orange vertical line represents the threshold voltage of +1.7 kV at which the extraction of ions began. After the applied voltage reached the threshold, the ion beam current began to increase linearly and became the steady state. The response delay as seen without the slew rate was not observed, and the response time was less than the order of nanoseconds.

4. Conclusions

We have conducted Particle-in-Cell simulations of electrospray thrusters using ionic liquid as the propellant and investigated the ion beam extraction mechanism in steady and transient flows.

Steady ion density and energy distributions were obtained in the simulation in addition to potential distributions. These distributions did not depend on whether ions contained only monomers or both monomers and dimers. Moreover, we evaluated the propulsion performance of the electrospray thruster. Then, the high specific impulse was obtained while the thrust per emitter was small. However, the thrust could be improved by increasing the number density of emitter cones.

The potential distribution with the jet was slightly changed in the vicinity of the emitter tip. Then, ion beam distributions with the jet were different from that without the jet, and the half angle of the ion beam was changed. However, additional analyses are necessary since the electrospray thruster model with the jet may be insufficient.

For the transient analysis, the ion beam current was found to change quickly when the polarity of the applied voltage was altered from +2 to −2 kV or from −2 to +2 kV. When the applied voltage with the finite slew rate was assumed, the quick response was also confirmed.

In the future, we will study ion motions at the emitter tip in more detail to determine the ion velocity and angular distributions thereat. In addition, we will integrate the simulation of the ionic liquid flow on the emitter surface and the ion beam extraction.

Acknowledgements

This work was financially supported in part by JSPS KAKENHI Grant Number JP15K14247 and the Asahi Glass Foundation. The part of the computer simulations was performed on the KDK computer system at the Research Institute for Sustainable Humanosphere, Kyoto University.

References

1) Watanabe, M.: Current and Future Scopes of Ionic Liquid Studies, *Surf. Sci. Soc. Jpn.*, **28** (2007), pp. 298-303 (in Japanese).
2) Takeuchi, M., Hamaguchi, T., Ryuto, H., and Takaoka, G. H.: Development of Ionic Liquid Ion Source with Porous Emitter for Surface Modification, *Nucl. Instruments and Methods in Phys. Res., Sec. B: Beam Interact. with Mater. Atoms*, **315** (2013), pp. 345-349.
3) Guerra-Garcia, C., Krejci, D., and Lozano, P.: Spatial Uniformity of the Current Emitted by an Array of Passively Fed Electrospray Porous Emitters, *J. Phys. D*, **49** (2016), pp. 115503-1-12.
4) Courtney, D. G., Dandavino, S., and Shea, H.: Comparing Direct and Indirect Thrust Measurements from Passively Fed Ionic Electrospray Thrusters, *J. Propul. Power*, **32** (2016), pp. 392-407.
5) Nakagawa, K., Tsuchiya, T., and Takao, Y.: Characteristics of Ion Beam Extraction for Ionic Liquid Electrospray Thruster, The 47th JSASS Annual Meeting, 1D06 (JSASS-2016-1061), 2016 (in Japanese).
6) Nakagawa, K., Tsuchiya, T., and Takao, Y.: Dependence of Beam Extraction Characteristics on Electrode Structures for Ionic Liquid Electrospray Thruster, The 60th Space Sciences and Technology Conference, P17 (JSASS-2016-4686), 2016 (in Japanese).
7) Nakagawa, K., Tsuchiya, T., and Takao, Y.: Microfabricated Emitter Arrays for an Ionic Liquid Electrospray Thruster, *Jpn. J. Appl. Phys.*, **56** (2017), pp. 06GN18-1-8.
8) Krpoun, R., Smith, K. L., Stark, J. P. W., and Shea, H. R.: Tailoring the Hydraulic Impedance of Out-of-Plane Micromachined Electrospray Sources with Integrated Electrodes, *Appl. Phys. Lett.*, **94** (2009), pp. 163502-1-3.
9) Hill, F. A., Heubel, E. V., De Leon, P. P., and Velasquez-Garcia, L. F.: High-Throughput Ionic Liquid Ion Sources Using Arrays of Microfabricated Electrospray Emitters with Integrated Extractor Grid and Carbon Nanotube Flow Control Structures, *J. Microelectromech. Syst.*, **23** (2014), pp. 1237-1248.
10) Emoto, K., Tsuchiya, T., and Takao, Y.: Numerical Investigation of Ion Beam Extraction Mechanism for Ionic Liquid Electrospray Thruster, The 60th Space Sciences and Technology Conference, P14 (JSASS-2016-4683), 2016 (in Japanese).
11) Birdsall, C. K. and Fellow, L.: Particle-in-Cell Charged-Particle Simulations, Plus Monte Carlo Collision with Neutral Atom, PIC-MCC, *IEEE Trans. Plasma Sci.*, **19** (1991), pp. 65-85.
12) Nicholls, A. and Honig, B.: A Rapid Finite Difference Algorithm, Utilizing Successive Over-Relaxation to Solve the Poisson–Boltzmann Equation, *J. Comput. Chem.*, **12** (1991), pp. 435-445.
13) Verboncoeur, J. P.: Symmetric Spline Weighting for Charge and Current Density in Particle Simulation, *J. Comput. Phys.*, **174** (2001), pp. 421-427.
14) Verboncoeur, J. P.: Particle Simulation of Plasmas: Review and Advances, *Plasma Phys. Control. Fusion*, **47** (2005), pp. A231-260.
15) Miller, S. W., Prince, B. D., Bemish, R. J., and Rovey, J. L.: Electrospray of 1-Butyl-3-Methylimidazolium Dicyanamide Under Variable Flow Rate Operations, *J. Propul. Power*, **30** (2014), pp. 1701-1710.
16) Lozano, P. C.: Energy Properties of an EMI-Im Ionic Liquid Ion Source, *J. Phys. D*, **39** (2005), pp. 126-134.
17) Nagao, M. and Yoshida, T.: Fabrication of Gated Nano Electron Source for Vacuum Nanoelectronics, *Microelectron. Eng.*, **132** (2015), pp. 14-20.
18) Inoue, N., Nagao, M., and Takao, Y.: Prototype of Electrospray Thrusters with High-Density Emitter Array Using Fabrication Technique of Field-Emission Electron Guns, The 48th JSASS Annual Meeting, 2D04 (JSASS-2017-1102), 2017 (in Japanese).
19) Dandavino, S., Ataman, C., Ryan, C. N., Chakraborty, S., Courtney, D., Stark, J. P. W., and Shea, H.: Microfabricated Electrospray Emitter Arrays with Integrated Extractor and Accelerator Electrodes for the Propulsion of Small Spacecraft, *J. Micromech. Microeng.*, **24** (2014), pp. 075011-1-13.